An Embedded, Eight Channel, Noise Canceling, Wireless, Wearable sEMG Data Acquisition System With Adaptive Muscle Contraction Detection

Mert Ergeneci, Kaan Gokcesu, Erhan Ertan, and Panagiotis Kosmas, *Senior Member, IEEE*

***Abstract*—Wearable technology has gained increasing popularity in the applications of healthcare, sports science, and biomedical engineering in recent years. Because of its convenient nature, the wearable technology is particularly useful in the acquisition of the physiological signals. Specifically, the (surface electromyography) sEMG systems, which measure the muscle activation potentials, greatly benefit from this technology in both clinical and industrial applications. However, the current wearable sEMG systems have several drawbacks including inefficient noise cancellation, insufficient measurement quality, and difficult integration to customized applications. Additionally, none of these sEMG data acquisition systems can detect sEMG signals (i.e., contractions), which provides a valuable environment for further studies such as human machine interaction, gesture recognition, and fatigue tracking. To this end, we introduce an embedded, eight channel, noise canceling, wireless, wearable sEMG data acquisition system with adaptive muscle contraction detection. Our design consists of two stages, which are the sEMG sensors and the multichannel data acquisition unit. For the first stage, we propose a low cost, dry, and active sEMG sensor that captures the muscle activation potentials, a data acquisition unit that evaluates these captured multichannel sEMG signals and transmits them to a user interface. In the data acquisition unit, the sEMG signals are processed through embedded, adaptive methods in order to reject the power line noise and detect the muscle contractions. Through extensive experiments, we demonstrate that our sEMG sensor outperforms a widely used commercially available product and our data acquisition system achieves 4.583 dB SNR gain with 98.9784% accuracy in the detection of the contractions.**

***Index Terms*—EMG sensors, noise cancellation, real-time data acquisition, wearable technology, adaptive systems, muscle contraction detection.**

I. Introduction

WEARABLE technology has gained a lot of attention in recent years because of its application in a wide range of fields such as gaming, medical analysis and human machine interface [1]–[15]. The various benefits of wearable technology include compactness, user-friendliness and continuous monitoring. Since wearable technologies can be used standalone, the experiments can be carried out in places other than laboratories [16]. The acquisition of muscle activity data particularly benefits from this since wearable data acquisition systems allow for a greater motion freedom [8], [15], [16].

In a wearable system, the muscle data is collected via electromyography (EMG) technology, which is an electrodiagnostic medicine technique for evaluating and recording the electrical activity produced by skeletal muscles [17]. EMG technology is used in a wide range of applications such as medical diagnosis and rehabilitation [18]–[21], sports science research, athlete monitoring [22], human machine interaction and gesture recognition [23]–[26]. Non-invasive EMG technology, i.e., surface electromyography (sEMG), has been recently used in research with these wearable systems [27].

Electrodes in sEMG sensors can be disposable (gel-based) or reusable (dry). Gel-based electrodes have a long setup time, are sensitive to long-term usage (motion) and are generally for single use [28]. Hence dry electrode technology is preferred for wearable applications. Although, active dry electrodes are readily available in the market, they are very expensive and are difficult to integrate into specific purpose systems [16], [28]. We have therefore designed an active, dry, low-cost sEMG sensor which can be integrated with an 8 channel data acquisition unit.

Our proposed sEMG data acquisition system hardware design consists of two parts, the sensors and the multi-channel data acquisition unit. In the first part (sensor), we amplify the sEMG signal that has a very low magnitude (0–5 mV) [29], [30]. The amplification process is designed to prevent noise and other disturbing artifacts [31]–[33]. After the amplification, an analog bandpass filter (20–500 Hz) is used to reduce the system noise and motion artifacts [34], [35]. Finally, the sensor outputs are connected to the second part of our system, which is an 8-channel data acquisition unit (DAU) that can capture up to 8 different sEMG signal streams simultaneously. In the second part of our system, i.e., DAU, the incoming sEMG channels are processed in a microcontroller unit (MCU)

Manuscript received April 8, 2017; revised July 17, 2017; accepted September 5, 2017. Date of publication November 3, 2017; date of current version January 26, 2018. This work was supported by the Scientific and Technological Research Council of Turkey under Project 2150287. This paper was recommended by Associate Editor D. Gangopadhyay. *(Corresponding author: Mert Ergeneci.)*

M. Ergeneci and E. Erhan are with Hercules Biomedical R&D, Ankara 06800, Turkey (e-mail: ergenecimert@gmail.com; erhertan@gmail.com).

K. Gokcesu is with the Department of Electrical Engineering and Computer Science, Massachusetts Institute of Technology, Cambridge, MA 02139 USA (e-mail: gokcesu@mit.edu).

P. Kosmas is with the School of Natural and Mathematical Sciences, King's College London, London WC2R 2LS, U.K. (e-mail: panagiotis.kosmas@kcl.ac.uk).

Color versions of one or more of the figures in this paper are available online at http://ieeexplore.ieee.org.

Digital Object Identifier 10.1109/TBCAS.2017.2757400

simultaneously. However, since the MCU can only process one waveform at a time, a multiplexer (MUX) is used to sequentially sample through all of the sEMG channels. After the processing at MCU, the sEMG signals are transmitted to an interface via WiFi. To exclusively acquire sEMG data, data is transmitted only when muscle activity/contractions are detected. To do this, we have introduced an embedded digital method to adaptively detect contractions. Through our adaptive contraction detection algorithm, the signals coming from the sEMG sensors are labeled according to their individual contraction and relaxation times, which lessens the complexity for data transmission as well (since only the parts of the signal including muscle activity are transmitted). This approach provides a valuable tool for further sEMG signal analysis such as in fatigue tracking, voluntary contraction ratio, muscle power development and muscle injury risk estimation since in order to perform most sEMG analyses only the contractions are required [16], [32], [36].

Moreover, in sEMG data acquisition, power line noise (PLN) is a huge obstacle that can reduce the captured waveform quality and make the analysis of the sEMG signals quite difficult [37]. Even though the PLN signal is known to be a sinusoidal at 50/60 Hz (possibly with its harmonics), its frequency can vary by ± 2 Hz and its amplitude is dependent on the environment (e.g., the power of electronic components) [30], [38]. To this end, we use an adaptive approach to minimize the adverse effects of PLN's frequency and amplitude variations. The algorithm is similarly embedded into the MCU located in the DAU. Most of the traditional approaches to reduce the PLN generally suffer from two significant problems, which are the loss of valuable EMG data near PLN frequency, and an inadequate decrease in the noise power due to nonadaptive structures [30], [36], [39], [40]. To overcome these limitations, we introduce an online adaptive algorithm which sequentially removes the power line noise whilst keeping the valuable EMG data untouched during active muscle periods.

The remainder of the paper is organized as follows. In Section II, we provide a detailed description of the state of the art in sEMG data acquisition systems, power line noise cancellation algorithms, and contraction detection techniques, as well as our design's contributions and improvements. Section III presents the overall hardware implementation of both the sEMG sensor and 8-channel data acquisition unit (DAU). Our contraction detection and noise cancellation methods are detailed in Section IV. In Section V, we present various experiments to validate the performance of our proposed sEMG data acquisition system. Experiments include the comparison of the proposed sEMG sensor with a commercially available product (Biometrics sx230–1000 [41]) by evaluating their respective SNR values and frequency responses during relaxation and contraction phases. We also include experiments for the error rate of our contraction detection algorithm and SNR gain of our noise cancellation method. Finally, some concluding remarks are given in Section VI.

II. Prior Art and Comparisons

In the academic literature and the industrial market, there are several solutions for sEMG data acquisition. These include the commercially available products Biometrics DataLOG [42], Delsys Trigno Lab [43], Myo Armband [27] and the academic works [28], [44]–[48]. The works in [28], [42], [48] lack wearability. Hence, they do not offer sufficient motion freedom. The solutions proposed in [44], [45], [47] do not use wireless data transmission and are not suitable for general use outside of laboratory environments. The works in [44], [48] use wet (disposable) electrodes, which do not offer reusability. The system in [28] supports only a single channel sEMG, which is insufficient for various sEMG applications. [27] only provides a sampling rate of 200 Hz, which is only suitable for detecting low frequency events (such as gestures) and cannot be used for general purpose EMG signal evaluations (such as fatigue tracking). Our system solves the various shortcomings of the current solutions to the sEMG data acquisition. A summary of the comparisons are given in Table I.

The systems proposed in [28], [42], [44], [45], [48] do not have any means of power line noise cancellation, which is especially problematic in high noise environments. On the other hand, the works in [27], [43], [46], [47] use notch filters, which are band-stop filters with a narrow bandwidth (located specifically at $50/60$ Hz and possibly at its harmonics). Adjusting the center frequency and the bandwidth of notch filters is not trivial. If the band is too small, it can miss the PLN frequency and a too large of a bandwidth can distort the valuable EMG data [30], [49]. To solve the data distortion problem of notch filters, Signal Interpolation method [49] have been proposed, which passes the observed EMG spectrum from a window smoothing (since it assumes that the observed spectrum is the superposition of the true EMG data and a peak at the PLN frequency). Laguerre filters [50] have been proposed as improved versions of the notch filters that solves the adaptivity issue. APF method [30], [51] iteratively estimates the frequency of the PLN and its harmonics. Regression Subtraction and Sinusoidal Modeling [30], [40] type approaches provide performance gains only if the PLN frequency is known in advance (since they try to fit a certain model). All of these methods (both adaptive or nonadaptive) aim to find the exact frequency and power of PLN. However, all of these methods substantially distort the valuable EMG data near PLN frequency because of overfitting. To this end, we propose a Q-learning based method to adaptively estimate the noise in the whole EMG spectrum, which subsequently removes only the stationary interferences including PLN (i.e., do not distort the valuable EMG signal).

Furthermore, our system can accurately detect the muscle contractions to acquire the sEMG data exclusively, which is nonexistent in the other systems. All of these systems merely provide the outputs of the sEMG channels. On the other hand, by detecting the time instances the sEMG data is present in the sEMG channel, we are able to truly perform sEMG data acquisition.

To detect contractions, various approaches in literature try to detect patterns in biosignals (EMG, ECG, EEG). As an example, various QRS detection techniques use successive thresholds to accurately capture and detect the specific signal behavior. They generally use a transform such as derivation to model the nonlinearity. In [52], [53], the authors approximate the derivative

TABLE I
COMPARISON OF THE SEMG DATA ACQUISITION SYSTEMS

Systems	Wearable	Contraction detection	Noise cancel.	Data trans.	Electrode Type / Material	Channels	Gain (V/V)	BW (Hz)	F_s (Hz)	ADC Res. (bits)
Hercules (this paper)	Yes	Yes	SE[1]	WiFi	Dry/Gold Plated Copper	8	500	20–500	1000	12
Biometrics datalog [42]	No	No	No	BLE	Dry/Stainless Steel	8	1000	20–460	1000	14
Delsys trigno [43]	Yes	No	Notch	RF	Dry/Silver	16	909	0–500	1926	16
Myo armband [27]	Yes	No	Notch	BLE	Dry/Stainless Steel	8	–	–	200	8
JPL V1 [44]	Yes	No	No	Wired	Wet/Silver Chloride	8	100	16–600	1000–2000	–
WB-EMG [28]	No	No	No	BLE	Dry/Gold Plated Copper	1	100–10000	20–450	1000	12
Paper [45]	Yes	No	No	Wired	Dry/Silver Plated Copper	8	100–1000	15–1000	1000	–
Paper [46]	Yes	No	Notch	RF	Dry/Silver Chloride	6	–	20–500	1000	10
Paper [47]	Yes	No	Notch	Wired	Dry/Silver Chloride	16	–	20–500	1000	–
Paper [48]	No	No	No	BLE	Wet/Silver Chloride	4	47–9588	8.7–952	4000	14

with a first order difference. In [54], the derivative is modeled with the difference of the low-pass filter output. In [55], the authors use an FIR filter to model the derivative. In all of these algorithms, the process outputs a nonnegative value (similar to a full-wave rectification), then the resulting output is compared with a threshold. Similarly, [56] proposes a matched filter on the Wavelet Transform of the signal to detect muscle activation. However, all of these techniques are used to recognize patterns in the signal, which requires the specific signal waveform a priori and have unsatisfactory performance in stochastic environments. To this end, [57] models the inactive and active signals as Gaussian processes with individual means and variances, and thresholds the likelihood ratio to produce a decision. The parameters of the inactive frames are calibrated at the beginning and the active part is calculated from the observations. However, in noisy environments (especially with PLN), erroneous estimations of these parameters may occur.

Henceforth, instead of detecting patterns, the general approach for detecting sEMG is to use a threshold on a certain metric of the sEMG data, which cumulatively captures its properties. Several metrics include Mean Absolute Value (MAV), Variance (VAR), Root Mean Square (RMS), Waveform Length (WL), Zero Crossing (ZC), Slope Sign Change (SSC), Discrete Wavelet Transform (DWT), Wavelet Package (WPT), Mean Frequency (MF), Median Frequency (MDF), Peak Frequency (PF), Mean Power (MP), Total Power (TP), Higuchi's Fractal Dimension (HFD), Detrended Fluctuation Analysis (DFA), Shannon Entropy (SE) [58]–[62]. However, most of them, especially the spectral metrics, can lead to incorrect representations of the sEMG signal under high noise and interference (e.g., PLN). Therefore, the most popular choice is to use RMS or some variant as the primary metric for determining whether there is a contraction. The general approach is to look at a limited bandwidth of the spectrum to determine the existence of contractions (generally with a low-pass or a band-pass filter) [63]. However, since PLN frequency overlaps with the bandwidth sEMG is most dominant, it can significantly degrade the performance of these metrics. To this end, we propose a new metric, which is based on the smoothed geometric mean of the power spectra. This metric highly deemphasizes the PLN power and is a suitable metric especially in high interference environments.

[1]Spectrum Estimation

Moreover, even though the general approach is to threshold a metric, the selection of this threshold is not trivial. [64] uses a predefined threshold, which is calibrated at the beginning of the measurements. Another technique is to set the threshold to the RMS of the last contraction and to compare this with the RMS of the incoming frames while incrementally decreasing it with a decay parameter. In [63], the authors calculate the 5% and 95% percentile RMS values and use a convex combination of them as threshold. In [65], the authors propose a peak detection algorithm, where the number of sEMG measurements above a selected threshold are determined to make a decision. The threshold is chosen as the closest peak to the max peak in a time frame. However, all of these approaches either perform unsatisfactorily or require the optimization of certain parameters for good performance. None of these techniques can adaptively select an appropriate threshold. To this end, we propose a truly sequential, completely adaptive and robust threshold selection scheme.

III. sEMG Data Acquisition System Hardware

In this section, we demonstrate the overall hardware implementation of the sEMG data acquisition system, from sensor design to user interface. In the first subsection (part A), we detail the sEMG sensor design (involving the electrode material and size selection) and the analog signal conditioning (amplification & filtering). In the second subsection (part B), the data acquisition unit (DAU) is described, which includes real-time digitalization of the signals coming from 8 different sEMG sensors, power supply and the wireless data transmission protocol to a user interface.

A. sEMG Sensor

The main purpose of the sensor is to amplify the electromyography signals to a meaningful range without significant distortion (e.g. motion artifact). Our sensor is composed of two basic parts, which are the electrode selection and the signal conditioning. We first start by explaining the electrode design and its optimal material selection.

1) Electrodes: The electromyography signals are received through the electrodes, which are conductive materials used for gathering and transferring the muscle activation potential [66]. The conductance of the material the electrodes are made of

TABLE II
SNR VALUE COMPARISON OF VARIED ELECTRODE TYPES

Material	Diameter	Thickness	SNR (dB)
Gold	6 mm	1 mm	29.0694
Gold	6 mm	2 mm	30.0365
Gold	10 mm	1 mm	35.1195
Gold	10 mm	2 mm	35.9704

plays a significant role in acquiring high quality sEMG signal. The commercialized metal that offers the highest conductance (i.e., the best quality) is silver [66]. However, since silver has a high market value, we have used copper as the main metal in our electrodes, which is highly affordable and offers high conduction similar to silver. The main problem with a pure copper electrode is its vulnerability to corrosion and oxidation. To this end, we have manufactured 100 nm gold-plated copper-core disk shaped electrodes since gold has a high resistance to corrosion and oxidation [66].

In order to determine the electrode that provides optimal performance, i.e., the best SNR value, we have tested various electrodes with different sizes. The electrode size is determined by two parameters, which are the electrode thickness and the surface area in contact with the skin. To compare the effect of size on SNR, we recorded data of gold-plated disk electrodes with diameter of 6 mm and 10 mm, and thickness of 2 mm and 1 mm. A larger electrode surface area increases the sensor contact with the body, leading to higher SNR. However, increasing the diameter of the electrode more than 10 mm causes noise and disturbance to the sEMG signal due to crosstalk and overrun of muscle fiber size [67]. Therefore, we avoided using electrodes with diameter more than 10 mm. Additionally, an increased thickness causes the electrodes to apply more pressure to the skin towards the muscle fibers, which also increases SNR, however, it may also create discomfort.

4 different types of electrodes were tested for 10 healthy subjects, and the average SNR values were calculated. Electrodes were placed to the biceps brachii, on the line between the medial acromion and the fossa cubit at $1/3$ from the fossa cubit of each individual [67]. The inner space between the electrodes (i.e., from center to center) was fixed to 20 mm[67].

The results of the experiment are demonstrated in Table II, which show that increasing the surface area and the thickness increases the SNR value. Thus, in our sEMG sensor design, we used gold plated disk electrode with 10 mm diameter, 2 mm thickness, since it demonstrated the best SNR, which is 35.9704 dB.

Next, we explain the signal conditioning, which involves amplification & filtering process of the raw muscle activity potential signals gathered from the electrodes.

2) Signal Conditioning: The electrodes collect and conduct the muscle signals, however, these signals in their raw form are not feasible to process. Since the collected muscle data from electrodes are very small in amplitude (less than 5 mV), the gathered signals are required to be amplified to a processable range, which is 0–3 V for our sensor.

The signals gathered in the electrodes are called V^+ and V^- individually. The sEMG signal is the potential difference of the signals that are collected from these electrodes. Let EMG_{amp} be the amplified sEMG signal, G_1 be the gain of the instrumentation amplifier and G_2 be the gain of the non-inverting amplifier. Then, the amplified sEMG signal is given by

$$EMG_{\text{amp}} = G_1 G_2 (V^+ - V^-). \tag{1}$$

The instrumentation amplifier calculates the potential difference between the electrodes V^+ and V^- and amplifies it [28], [34], [68]. In our circuitry, we used $AD8221$ as the instrumentation amplifier, which is very low-power and has high common mode rejection ratio (CMRR). CMRR is a very significant value for instrumentation amplifiers since it shows the attenuation amount of common mode, which reduces the power line noise [69]. We set the instrumentation amplifier gain, i.e., G_1, to 50.

Secondly, DC offset levels of the signal coming from the electrodes generally differ due to the displacement caused by the skeletal motion during contraction [16], [35], [68]. This varying DC level of V^+ and V^- electrodes cause a huge DC offset at the output of the instrumentation amplifier since $AD8221$ takes the difference of the voltage values of the electrodes and multiplies it with a gain of $G_1 = 50$. In order to prevent amplification of this DC offset, we generated an AC coupling quasi-high pass filter with the use of a 220 uF capacitor placed between the RG pins (i.e., 2,3) of the instrumentation amplifier. By this simple RC filter, $AD8221$ outputs a zero-mean sEMG signal to the gain part.

To obtain a total gain of 500, we divided the gain into two parts: an instrumentation amplifier gain, $G_1 = 50$, followed by a simple non-inverting amplifier circuit via an $OP777$ with a gain, $G_2 = 10$. The photo of the amplification circuitry PCB is given in Fig. 1-a.

The last stage of the sEMG sensor is the filtering part, where the amplified signal is processed prior to the data acquisition unit (DAU). The photo of the filter circuitry PCB is given in Fig.1-b. The incoming signal is filtered through a bandpass filter with a band of 20–500 Hz. The bandpass filter used is a cascaded design of a high pass filter followed by a low pass filter.

According to ISEK standards, EMG signal components at frequencies below 20 Hz are caused by motion artifacts due to the skeletal movement of the muscle during contractions and the electrode-skin interface [34], [35]. In order to prevent the motion artifact, we designed a high-pass filter with a cut-off frequency of 18 Hz. The designed filter has a Sallen-Key filter topology with a Butterworth response. Additionally, the corner frequency attenuation is 3 dB and the stopband frequency attenuation is 20 dB.

EMG signal is recommended to be sampled with a sampling frequency of 1 kHz according to ISEK and SENIAM, i.e., EMG signal does not exceed 500 Hz, which enables us to reduce noise by filtering out the frequency components (noise) above 500 Hz [28], [34]. The designed filter has a multiple feedback circuit topology with a Butterworth response. In order to have a stopband frequency at 500 Hz, cutoff frequency is selected to be 290 Hz. Also, the corner frequency attenuation is 3 dB and stopband frequency attenuation is 20 dB.

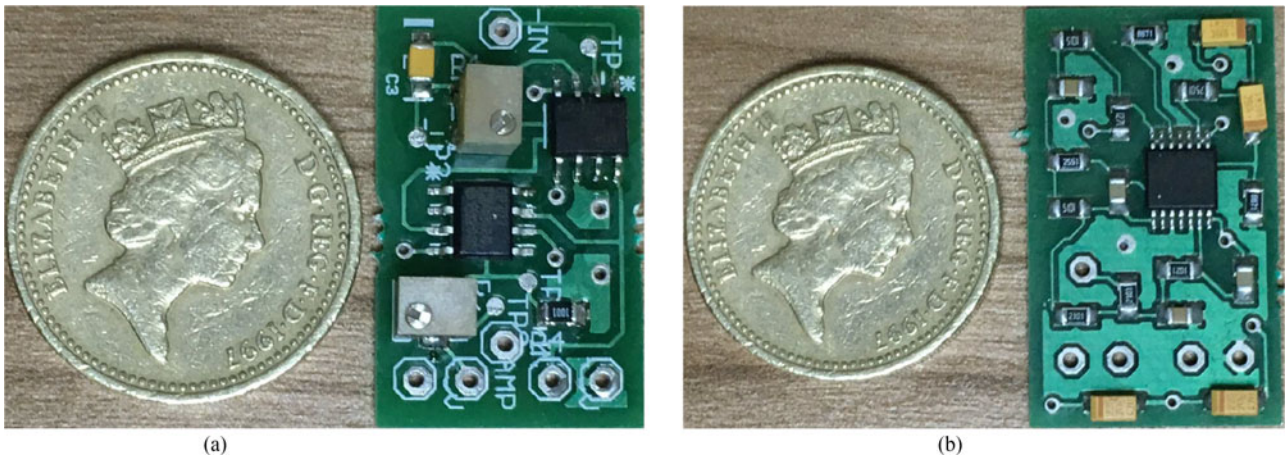

Fig. 1. (a) Photo of the amplification circuitry PCB. (b) Photo of the filter circuitry PCB.

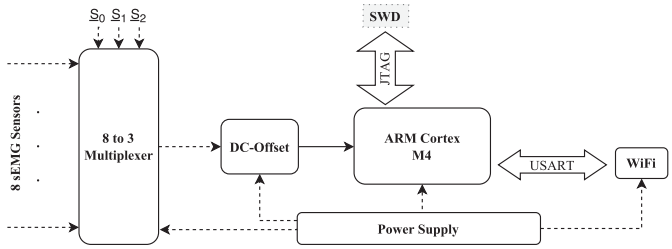

Fig. 2. Overall sEMG data acquisition unit block diagram.

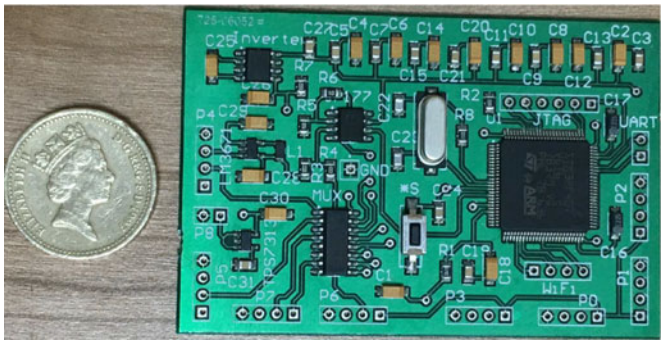

Fig. 3. Photo of the eight channel sEMG data acquisition unit (DAU) PCB.

In the next subsection, we detail the 8-channel sEMG data acquisition unit (DAU) that uses 8 of the sensors described in this section as inputs.

B. 8 Channel sEMG Data Acquisition Unit (DAU)

The sEMG data acquisition unit (DAU) mainly collects the signals coming from the sEMG sensors and transmits the incoming information with WiFi protocol. The incoming signals are converted to digital and passed through certain adaptive signal processing methods, which are the contraction detection (Section IV-A) and the noise cancellation (Section IV-B). Then, the sensor data is transmitted to a device (i.e., computer or mobile phone) via WiFi (UDP protocol).

The block diagram and the photo of the circuitry PCB of the overall data acquisition unit are given in Fig. 2 and Fig. 3, respectively. The system is composed of five main stages, which are multiplexer (MUX), DC-Offset, micro controller unit (MCU), power supply and data transmission (WiFi).

The first stage of DAU, i.e., MUX creates the multi-channel architecture. The 8 different sEMG channels enter the MUX where they are transferred to the DC-Offset unit sequentially. Since the sEMG signal band ranges between 20–500 Hz, it is required to sample the incoming signals with a sampling rate of minimum 1 kHz, which corresponds to a maximum of 1 ms period.

Thus, we decided to change the select pins (i.e., S_0, S_1, S_2) of the MUX with a clock of 8 kHz which would lead to a 1 ms delay (1 kHz sampling frequency) between each sEMG signals' individual samples. In this way, we prevent any data loss and collect 8 different incoming sEMG signals simultaneously.

The select pins (S_0, S_1, S_2) of the MUX are controlled by the MCU and the output of the MUX is directly connected to the DC-Offset module where 1.5 V DC-Offset is added to the signal. The DC-offset module converts the zero-mean signal to a unipolar signal with a range of 0–3 V to suitably interface with the ADC in the ARM Cortex CPU. A Unipolar ADC cannot convert negative voltage values. Thus, we up-shifted the mean of the EMG signal to 1.5 V, which positions the signal inside the ADC voltage range. After the addition of DC-Offset, the signals are digitalized in the internal ADC of the MCU. We used an ARM cortex-M4 based, $stm32f407vgt6$, microcontroller. The MCU requires external crystal (8 MHz) and a power supply circuit. It is possible to program the MCU through SWD pins via an external ST-LINKV2 debugger. The sEMG signals coming from the DC-Offset unit are first converted to digital and stored in arrays in accordance with the select of that time instance since each select value corresponds to a different sensor.

Then, the digital data in arrays are cleaned from noise and the contraction (active) frames are detected in an adaptive manner. The cleaned contraction frames of signals are sent to WiFi module with USART protocol for transmission purposes. We emphasize that only the active frames are transmitted through WiFi in order to truly acquire the sEMG signals.

Power supply unit (PSU) is composed of a battery (3.7 V LiPo, 700 mA), regulators and an inverter. PSU supplies 3 V to

the DAU for MUX, DC-Offset, MCU, WiFi and an additional 1.5 V for again DC-Offset. Moreover, sEMG sensors, which are fed by the DAU, require ± 3 V supply for both amplification and filtering. Thus, in total, 3 V, -3 V and 1.5 V are required for the overall system and are supplied by PSU.In the PSU, 3 V is obtained by the $TPS73130$ regulator, 1.5 V is created using $LM3671$ regulator and -3 V by the $ICL7660$ inverter.

Lastly, data transmission is realized through WiFi module $RN171$. The data to be transmitted is sent to the WiFi module via USART protocol by MCU. Since 8 different sEMG signals are sampled with a 12-bit ADC (which is sufficient according to SENIAM standards [28]), 3 bytes of data is needed to be sent in order to transmit a sEMG sample correctly, where the first byte tells the channel number of the data (i.e., select pin of the MUX), other two bytes carry the 12-bit information (6 bits each with 2 bits of opcode showing the high and low part). In order to send 8 different sEMG data without any loss, baud rate is selected to be 230400.

In the following section, we explain the digital methods (contraction detection and noise cancellation) implemented in the MCU.

IV. Embedded Methods

In this section, we introduce two adaptive digital algorithms, which are applied to the sEMG signals inside the MCU. Firstly, the adaptive contraction detection algorithm detects if a contraction is present in the sEMG signal, and uses this information to decide whether to transmit the signal to the user interface. Secondly, the adaptive noise cancellation algorithm adaptively learns the PLN and removes it from the received sEMG signal. The continuous sEMG signal streams are split into frames of L samples (e.g., 255) sequentially with an overlap of W (e.g., 127). Both of the proposed methods processes these signal frames. In the following subsections, we explain these adaptive algorithms in detail.

A. Adaptive Contraction Detection

The main purpose of this method is to determine whether the incoming sEMG frame contains a contraction. Since the sEMG contraction times are not necessarily provided in most sEMG applications, it is required to classify the types of frames (contraction or relaxation) for applications such as PLN cancellation and fatigue detection [16], [32], [36]. The sEMG contraction and relaxation power are highly dependent to the subject using the sensor, sensor specifications (i.e., amount of amplification), the type of muscle group and the noise in the environment [30], [38]. Thus, it is beneficial to use an adaptive approach in frame classification.

1) Feature Creation: In order to determine whether the received frame involves contraction or relaxation data, we use the geometric mean of the received frame's power spectra as our comparison metric (i.e., feature). Assume x_n is the nth received frame, which is a column vector of length L, of the incoming sEMG data stream, then X_n is the K-point Fourier Transform of x_n, which is a column vector of size K (total number of frequency bins). The Spectral Power I_n is calculated from X_n as

$$I_n = \underbrace{(X_n \circ X_n)}_{\text{Hadamard product}} . \tag{2}$$

Traditionally, the arithmetic mean of the power spectra is used to determine the presence of a contraction since it corresponds to the signal power. However, we use the geometric mean instead of the arithmetic mean to decrease the dependency of the comparison metric on the noise in relaxation (inactive) frames. Since the inactive frames only contain PLN, at 50/60 Hz, and AWGN at all the frequency bins, the effect of the PLN component on the overall energy shows high dominance over any other component. Note that the PLN may show gradual change in amplitude in accordance with the environment. Hence, using arithmetic mean as the comparison metric would prove to be inefficient in environments with highly varying PLN, which may lead to misclassification of frames. On the other hand, geometric mean calculations ignore (highly attenuate) the effect of a single component (e.g., power at $50/60$ Hz) on the overall mean, e.g., if only $I_n[i]^{\frac{1}{K}}$ changes, then the geometric mean G_n will approximately stay the same for sufficiently high K. If the power is distributed amongst a wider frequency bandwidth (e.g., the spectrum of contraction as opposed to the PLN), its geometric mean will be higher. Because of its concavity, geometric mean function favors distributions closer to uniform distribution. Thus, the distinction between contraction and relaxation would be emphasized, which creates a better feature for classification. Hence, we compute the geometric mean, G_n, of the spectral power I_n as

$$G_n = \left(\prod_{i=1}^{K} (I_n[i] + 1) \right)^{1/K} , \tag{3}$$

where we also used an additive smoothing factor of 1. The reason for smoothing (adding) the power spectra with 1 is to prevent the possible adverse effects of the AWGN noise. It is possible for the noise power at a certain frequency bin to be really close to zero, which can in turn make G_n really low if the geometric mean was implemented directly. However, with this smoothing parameter, G_n is guaranteed to be greater than or equal to one. Even though geometric mean of the power spectra have similar values for relaxation frames (i.e., creates a stable comparison metric), it is still insufficient in creating similar values for contraction frames. Thus, we create the feature

$$\Psi_n = \log G_n . \tag{4}$$

This new feature, Ψ_n, in (4) de-emphasizes the high values of G_n and assigns closer values to contraction frames by attenuating the huge variations in geometric means of active frames. The algorithm decides whether the received sEMG frame contains a contraction by comparing it with a dynamic threshold. Next, we show how this threshold can be adaptively selected.

2) Threshold Update: It is known that the acquired sEMG signal is the superposition of electromyography signals released from measured muscle and noise including the PLN. When there is no contraction, i.e., during relaxation, the acquired sEMG signal is only noise which corresponds to the AWGN along

with the PLN. To this end, we classify the received sEMG frames through an adaptive thresholding approach on Ψ_n.

The selection of the threshold, τ_n, is very critical since the type of the received frames would be decided according to τ_n such that $\Psi_n > \tau_n$ would be a contraction and $\Psi_n \leq \tau_n$ a relaxation. However, the power levels of contraction and relaxation frames show a significant change according to the subject using the sensor, thus, using a predetermined τ_n is not possible. Hence, we learn and update the threshold level in an online manner with a moving average update. However, simply averaging the features Ψ_n to determine τ_n would prove to be insufficient since the averaging would provide an undesirably large value. Instead, we choose to do this moving average update in a different kernel space. We can generalize the moving average calculation in accordance with a selected kernel function $\Phi(\cdot)$ as

$$y_n = \Phi^{-1}\left(\frac{1}{N}\sum_{t=n-N}^{n-1}\Phi(x[t])\right), \tag{5}$$

where N is the length of the moving average window, $x[t]$ are the inputs (e.g., Ψ_t features) and y_n is the output (e.g., τ_n) at frame n.

The kernel function, $\Phi(\cdot)$ should be chosen carefully since the learning is unsupervised, which suggests that there is no reference showing if the received frame is contraction or relaxation. Since the numeric difference between the contraction and relaxation frames is high, the selected kernel function requires to be closer to the level of relaxation frames in order not to classify some small contractions as relaxation.

Hence, we choose the negative exponential as our kernel function such that

$$\Phi(x) = e^{-x} \tag{6}$$

It is seen that the negative exponential transform of Ψ_n is used in order to prevent undesirably high mean from the accumulation of gradual contractions. Since using negative exponential lowers the threshold level, $\tau*$ would approach to the minimum bounds, i.e., even after plenty of gradual and maximal muscle activations, a small contraction would be detected correctly. Additionally, the use of this kernel function effectively ignores any offset in the features Ψ_n, i.e., if all the features were offset by a constant c, the threshold found from the moving average in (5) will also be offset by the same constant c.

We note that (5) can be written in a recursive form. Hence, the update of τ_n, which is made through a moving average in accordance with the mean function $\Phi(\cdot)$ can be written as

$$\tau_{n+1} = \Phi^{-1}\left(\Phi(\tau_n) + \frac{1}{N}\left(\Phi(\Psi_n) - \Phi(\Psi_{n-N})\right)\right). \tag{7}$$

When the threshold update calculation in (7) is computed using the kernel function in (6) and its inverse, the update equation becomes

$$\tau_{n+1} = -\log\left(e^{-\tau_n} + \frac{1}{N}\left(e^{-\Psi_n} - e^{-\Psi_{n-N}}\right)\right), \tag{8}$$

where $-\log(\cdot)$ corresponds to the inverse mapping, i.e., $\Phi^{-1}(\cdot)$.

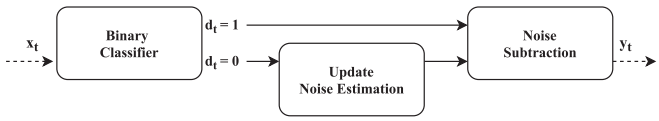

Fig. 4. Adaptive noise cancellation methodology.

3) Decision: After the threshold is determined adaptively in an online manner, the decision of the nth received frame, d_n, is computed as

$$d_n = \begin{cases} 1, & \Psi_n > \tau_n \text{ (contraction)} \\ 0, & \Psi_n \leq \tau_n \text{ (relaxation)} \end{cases}, \tag{9}$$

i.e., if the received frame is contraction, d_n is assigned to be 1 and 0 otherwise.

Determining the type of frames would lead to a true acquisition of the sEMG signal. Additionally, the decision value, d_n, is used in the noise cancellation (as explained in IV-B), since the inactive signal spectrum estimation requires only the frames involving noise (i.e., full relaxation involves only noise) for a proper noise subtraction. Moreover, these decisions d_n can be used in further applications such as fatigue level tracking, injury prevention and muscle development. Next, we explain our adaptive noise cancellation algorithm that can remove the PLN in an online manner.

B. Adaptive Noise Cancellation

In this section, we introduce an online adaptive noise canceling method that significantly reduces the PLN.

As seen in Fig. 4, incoming sEMG signal frames are first passed through a binary classifier in order to determine if the received frame is contraction or relaxation. The methodology of the binary classifier is described in IV-A. Then, if the sEMG window is a relaxation, i.e., $d_t = 0$, the noise spectrum estimation is updated by using the incoming relaxation frame (i.e., noise) and the new estimate is subtracted from the received frame. On the other hand, if $d_t = 1$, the estimation is directly subtracted from the received frame without any update. After the subtraction, noise-free sEMG signal frame is obtained. The overall noise signal may show a change since the PLN frequency can vary ± 2 Hz and its amplitude is highly dependent to the power of the nearest electronic components, the placement of the sensor, the subject using the sensor and the skin-electrode interaction [30], [38]. Hence, the estimated noise should be updated with each received relaxation frame. In the following subsections the update of the noise spectrum estimation and subtraction of the estimated noise are described respectively.

1) Update of the Noise Spectrum Estimation: In this part, we estimate the frequency spectrum of the overall noise signal and update it along with any further incoming noise frames. To do this, the received signal needs to include only noise, which corresponds to the relaxation frames. Since in IV-A, we introduce an adaptive method for classifying contraction and relaxation frames, it would be useful to consider only the frames that output $d_n = 0$ from the binary classifier in (9).

After receiving an inactive frame, the Discrete Fourier Transform (DFT) of the window is taken. In order to lessen the

TABLE III
INFORMATION ABOUT GENDER, AGE, HEIGHT AND WEIGHT OF THE SUBJECTS

Subject no	Age	Gender	Height (cm)	Weight (kg)
S1	20	Female	167	61
S2	24	Female	169	67
S3	26	Female	165	58
S4	24	Male	173	72
S5	25	Male	178	68
S6	28	Male	168	70
S7	24	Male	167	72
S8	25	Male	189	66
S9	24	Male	175	78
S10	24	Female	181	60

computation complexity, we only consider the first half of the DFT transform due to the symmetry for real signals. The calculated spectrum is updated using an exponential update with parameter α. Let P_n be the estimated noise spectrum of the nth frame and $\tilde{X}_n$ be the phase-shifted spectrum of the received relaxation frame. Then, the calculation of the updated spectrum, P_{n+1} is given by

$$P_{n+1} = (1-\alpha)P_n + \alpha\tilde{X}_n. \tag{10}$$

In the update method shown in (10), $\tilde{X}_n$ is used in order to prevent any miscalculation due to the phase difference of the incoming relaxation frame X_n. Since the phase values of X_n and P_n may differ, we synchronize their phases such that

$$\tilde{X}_n[k] = X_n[k]e^{(-jk\phi_n)}, \tag{11}$$

where k is the frequency bins of the whole spectrum, and ϕ_n is the phase difference between X_n and P_n. We can find the phase difference ϕ_n from a reference frequency point, e.g., the frequency index of the PLN, which is $50/60$ Hz depending on the region. Thus, ϕ_n is calculated as

$$\phi_n = \frac{1}{f}\left(\psi(X_n[f]) - \psi(P_n[f])\right),$$

where f is the PLN frequency index and $\psi(\cdot)$ is the phase function for a complex variable.

2) Subtraction of Estimated Noise: In this subsection, the estimated noise is converted to time-domain and subtracted from the received frame whether the frame involves contraction or relaxation signal. Before subtraction, the estimated noise spectrum is again phase-shifted in accordance with the received frame similar to (11). Then, the phase-synchronized version of the noise spectrum estimation is converted to time-domain by taking its inverse DFT. Finally, the time-domain estimation of the noise signal is subtracted from the received sEMG frame, which creates the noise-free sEMG signal window.

V. EXPERIMENTS

We have conducted three main experiments to test and validate our sEMG data acquisition system performance. All sEMG recordings are made from the biceps brachii, on the line between the medial acromion and the fossa cubit at $1/3$ from the fossa cubit [67]. In the experiments, sEMG data is captured from 10 different subjects with varied gender, age, weight and height properties as seen in Table III. The subjects are split into two groups. The first group (involving subjects $S1$ to $S5$) fixed their arm at a 90-degree position and realized repetitive, approximately 1 second long, maximal dynamic contractions with approximately 1 second relaxations in between. The second group (involving subjects $S6$ to $S10$) realized completely random contractions with independent timing, contraction amount and arm movement. All sEMG recordings lasted approximately 150 seconds. The reason for applying varied contraction procedures, which are visualized in Fig. 5, is to create a medium for evaluating, validating and testing proposed digital and analog applications of the overall system in different scenarios.

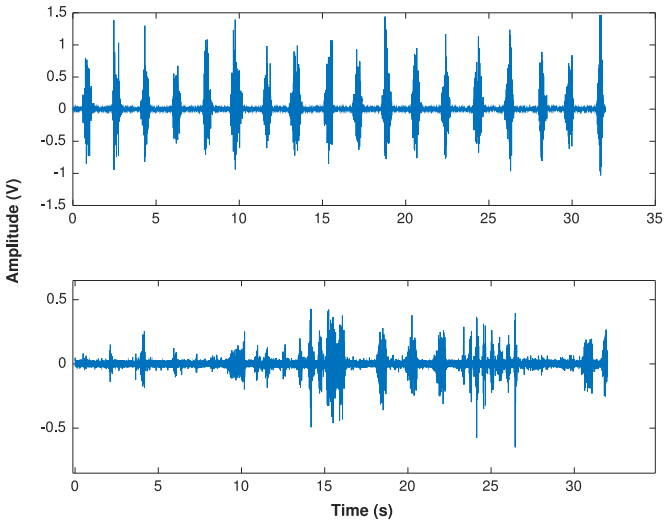

Fig. 5. Plots of the selections of the sEMG signal stream of S2 from the group 1 (top) and S9 from the group 2 (bottom).

In Section V-A, we compared the signal acquisition quality of the proposed sEMG sensor to the commercially available product Biometrics sx230–1000 [41]. In Section IV-A, we analyze the performance of the contraction detection algorithm along with its error rates. Finally, in Section V-C, the effect of the noise cancellation algorithm, i.e., its SNR gain, is observed. All the experiments are realized in MatLab 2016b.

A. Validation of the Sensor

In this part, the data acquisition quality of the proposed sensor design in Section III is tested and compared to a commercial, dry, active sEMG sensor Biometrics sx230–1000. The characteristics of an sEMG signal can be analyzed through time and frequency domain evaluations. Thus, we used SNR (time-domain) and DFT plots (frequency-domain) as our comparison tools. DFT plots show the filtration characteristics and frequency accumulation of the sEMG signal. On the other hand, SNR demonstrates the quality of signal waveform as opposed to the overall system noise interference. Since an objective comparison of the two sensors requires the sEMG recordings to be made under equal circumstances, we used Group 1 along with the described contraction procedure.

In Table IV, it is clearly seen that both of the devices capture approximately same amount of muscle signal and noise, resulting in very close SNRs. However, our sensor (Hercules) outperformed Biometrics with an extra 1 dB SNR gain.

TABLE IV
SIGNAL POWER, NOISE POWER AND SNR COMPARISONS OF BIOMETRICS AND HERCULES

	Signal power (dB)	Noise power (dB)	SNR (dB)
Biometrics	44.4183	8.8483	35.5700
Hercules	43.8804	7.1813	**36.6991**

TABLE V
FALSE POSITIVE, FALSE NEGATIVE, TOTAL ERROR AND CORRECT DECISION AMOUNTS AND PERCENTAGES

	False +	False −	Error	Correct
Amount	23	3	26	2519
Percentage	0.9037	0.1179	1.0216	98.9784

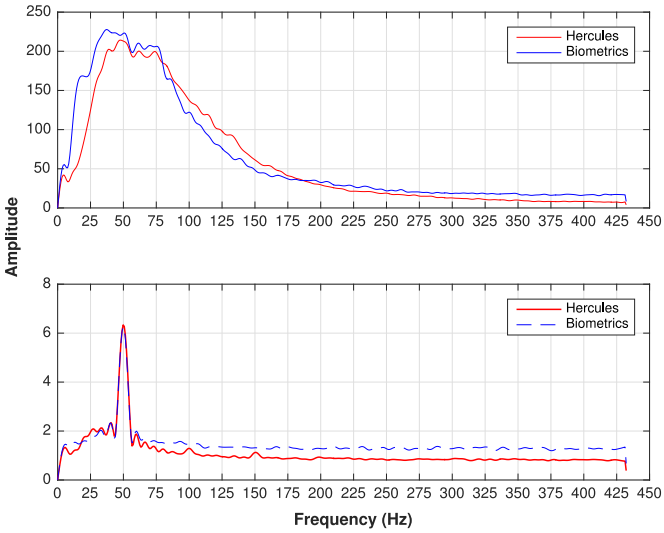

Fig. 6. Average frequency spectrum comparisons of contraction (top) and relaxation (bottom) frames of Biometrics and Hercules.

Moreover, in order to validate the analog signal processing quality (i.e., filtration), we compared the average DFT plots of the data that is gathered from Group 1. In this part, the received sEMG data for both devices, i.e., Biometrics and Hercules, are classified as contraction and relaxation frames and the DFTs of the classified frames are taken and averaged separately. As shown in Fig. 6, both sensors, during contractions, exhibit more dense spectra in the 20–150 Hz region, which corresponds to the anticipated sEMG frequency accumulation.

Furthermore, the 20–500 Hz band-pass filter impact can be clearly seen from the average DFT plots. In the average contraction DFT plot, the proposed sensor design, compared to Biometrics, shows a more strict decline after 300 Hz and before 25 Hz, which is one of the key factors resulting in a lower noise power (on average 1.6 dB) and a higher SNR (on average 1.1 dB).

B. Validation of the Contraction Detection Algorithm

In this section, the adaptive contraction detection algorithm is tested via the random data recorded from Group 2, i.e., $S6 - S10$. All the subjects realized 150 seconds long random contractions as described in Section V. The recorded sEMG signals are sent through the contraction detector, in which the signal stream is split into frames of 255 and a decision is made (i.e., contraction or relaxation). All the decisions are compared with a true threshold, which is calculated sample by sample by visual inspection. In Table V, the overall comparison of adaptive threshold and true threshold is shown. If a relaxation frame is received and the proposed algorithm decides that the frame contains contraction, the system gives a false positive error, which does not cause any critical problems. On the other hand, a false negative, which happens when the algorithm classifies a received contraction frame as relaxation, is the error that is very critical and may lead to sEMG signals' incomplete transmission since DAU sends only the contraction frames in order to truly acquire the sEMG data.

As seen in Table V, the false negative (false −) amount is 3, which means only 3 contraction frames are classified as relaxation among 2545 windows. Secondly, most of the false positive errors are realized in the beginning of the classification, where the adaptive thresholding was still in the early learning stages.

In Fig. 7, it is seen that only in the beginning, the adaptive threshold misclassifies the received frames, which means that most of the errors that are shown in Table V are due to the calibration of the contraction detection algorithm. Additionally, in order to demonstrate the sensitivity of the proposed algorithm, very small contractions between 225th and 290th frames are magnified and displayed in Fig. 7. Fig. 8 illustrates that even very low contractions (approximately $100mV_{p-p}$) made in a noisy platform (approximately $70mV_{p-p}$) are detected and picked out successfully by our algorithm.

C. Validation of the Noise Cancellation Algorithm

In this part of the experiment, sEMG data from all the subjects, i.e., Group 1 and 2, are evaluated since the noise cancellation algorithm does not require any specific contraction procedure for validation. To begin with, after the application of the noise cancellation algorithm, the average SNR gain of 4.583 dB is obtained, which is mostly due to the 4.61 dB average decrease in the noise power. Also, the overall decrease in the signal power is only 0.27 dB, which suggests that the valuable sEMG contraction data loss is extremely low.

In Fig. 9, the average spectrum of the noise frames before and after the noise cancellation are illustrated. It is seen that the noise is successfully estimated since noise at the PLN frequency (i.e., 50 Hz) is decreased approximately 15 dB and the subbands are perfectly rejected. Also, the difference of the output and the input of the noise cancellation algorithm (i.e., the second plot in Fig. 9) gives the estimated spectrum of the noise. Since it highly resembles the average noise spectrum, it suggests that our estimation is successful.

In Fig. 10, the average spectrum of the contraction frames is displayed in order to show that our algorithm does not disturb the valuable sEMG contraction signal.

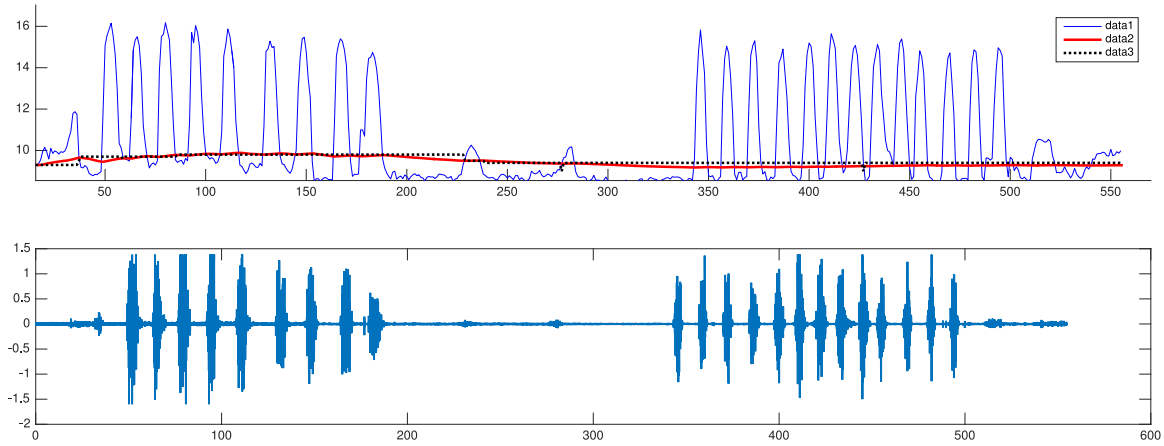

Fig. 7. Plots of contraction detection classifier, adaptive threshold and true threshold of subject S7 (above) and plot of recorded sEMG signal (below).

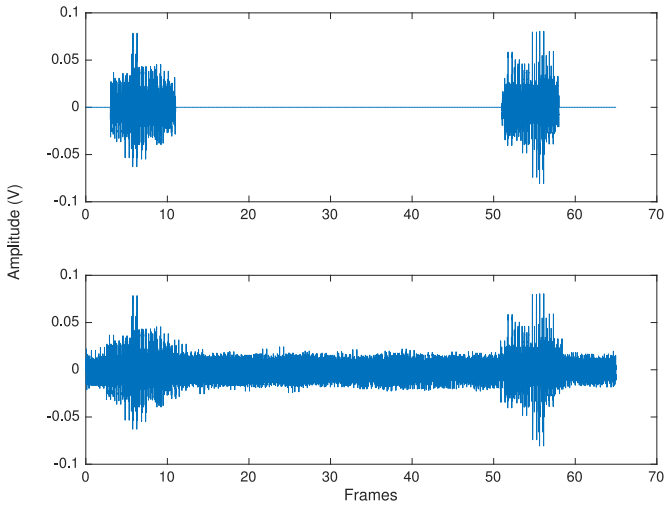

Fig. 8. Part of the received sEMG signal before (bottom) and after (top) the contraction detection algorithm.

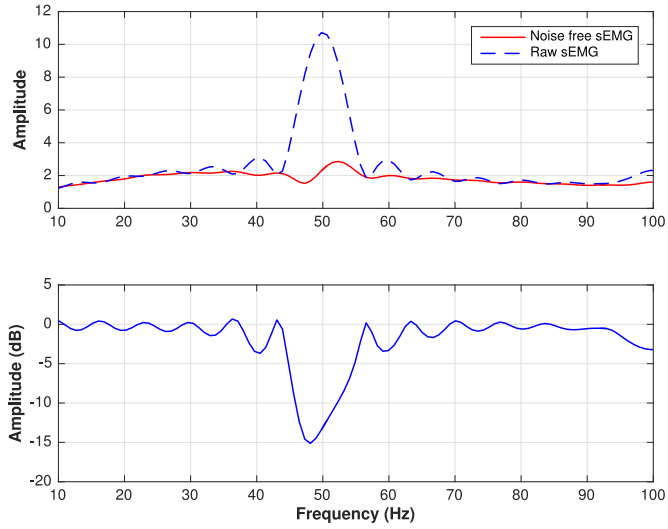

Fig. 9. Average noise frequency spectrum of cleared and raw sEMG signals (above) and the difference of those signals in dB scale (below).

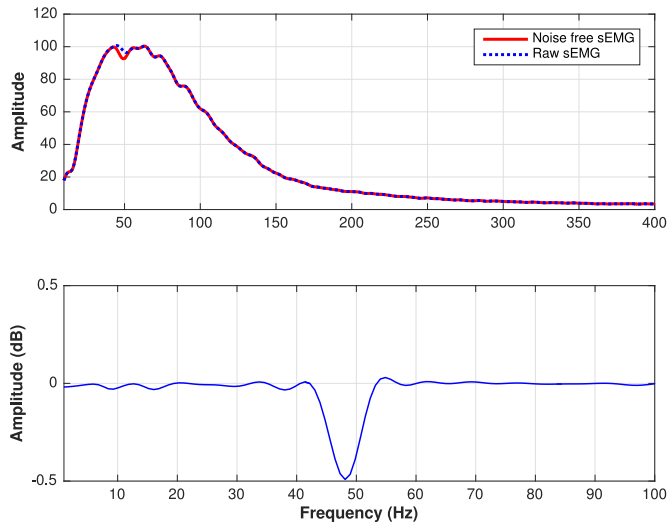

Fig. 10. Average contraction frequency spectrum of cleared and raw sEMG signals (above) and the difference of those signals in dB scale (below).

VI. Conclusion

In this paper, we proposed a successful implementation of a dry, active, noise canceling, low cost and wearable 8-channel sEMG data acquisition system along with two embedded digital methods, which are the adaptive contraction detection and the noise cancellation. We compared the performances of our sEMG sensors with the commercially available product Biometrics sx230–1000 in terms of SNR values and frequency spectrum analysis. In our comparisons, we illustrated that our low cost sensors showed high similarity in its signal waveform quality with Biometrics. Hence, the data acquisition performance of the Hercules sensor is validated since it demonstrated similar frequency band accumulation, overall 1.1 dB more SNR and a more strict band-pass filtration (20–500 Hz) than Biometrics sx230–1000.

Moreover, the presented adaptive contraction detection algorithm successfully decides if the received sEMG frame involves contraction or relaxation. Such classifications would make it possible for exclusive acquisition of sEMG data, which

consequently lessens the data transmission and the analysis complexity for further sEMG signal evaluations such as muscle fatigue tracking, muscle contraction rate and muscle power development. Thus, transmitting only the contraction signals creates an efficient tool for better sEMG signal processing.

We also demonstrated that our online adaptive power line noise (PLN) cancellation algorithm, which estimates the spectrum of the noise signal and subtracts the estimation from the received sEMG frames, successfully cancels the noise components in the received sEMG signal.

Thus, we have proposed an sEMG data acquisition system, which cancels PLN (-15 dB on average at the PLN frequency) without any critical disturbance to the sEMG signal (-0.5 dB on average at the PLN frequency), detects contraction with 98.9784% success rate, truly acquires sEMG data with high quality and can be straightforwardly integrated to any wearable device. Future work will focus on the design of a wearable product (sportswear) that analyzes the elite athlete training performance in real-time.

REFERENCES

[1] S. Benatti, B. Milosevic, E. Farella, E. Gruppioni, and L. Benini, "A prosthetic hand body area controller based on efficient pattern recognition control strategies," *Sensors*, vol. 17, no. 4, pp. 2-17–4-17, 2017.

[2] S. L. Teng, R. Rieger, and Y. B. Lin, "Programmable EXG biopotential front-end IC for wearable applications," *IEEE Trans. Biomed. Circuits Syst.*, vol. 8, no. 4, pp. 543–551, Aug. 2014.

[3] A. B. M. S. U. Doulah, S. A. Fattah, W. P. Zhu, and M. O. Ahmad, "Wavelet domain feature extraction scheme based on dominant motor unit action potential of EMG signal for neuromuscular disease classification," *IEEE Trans. Biomed. Circuits Syst.*, vol. 8, no. 2, pp. 155–164, Apr. 2014.

[4] A. M. R. Dixon, E. G. Allstot, D. Gangopadhyay, and D. J. Allstot, "Compressed sensing system considerations for ECG and EMG wireless biosensors," *IEEE Trans. Biomed. Circuits Syst.*, vol. 6, no. 2, pp. 156–166, Apr. 2012.

[5] E. Mastinu, P. Doguet, Y. Botquin, B. Hkansson, and M. Ortiz-Catalan, "Embedded system for prosthetic control using implanted neuromuscular interfaces accessed via an osseointegrated implant," *IEEE Trans. Biomed. Circuits Syst.*, vol. 11, no. 4, pp. 867–877, Aug. 2017.

[6] T. Morrison, M. Nagaraju, B. Winslow, A. Bernard, and B. P. Otis, "A 0.5 $rmcm^3$ four-channel 1.1 mw wireless biosignal interface with 20 m range," *IEEE Trans. Biomed. Circuits Syst.*, vol. 8, no. 1, pp. 138–147, Feb. 2014.

[7] S. J. Thomas, R. R. Harrison, A. Leonardo, and M. S. Reynolds, "A battery-free multichannel digital neural/EMG telemetry system for flying insects," *IEEE Trans. Biomed. Circuits Syst.*, vol. 6, no. 5, pp. 424–436, Oct. 2012.

[8] H. Lewy, "Wearable technologies—Future challenges for implementation in healthcare services," *Healthcare Technol. Lett.*, vol. 2, no. 1, pp. 2–5, 2015.

[9] A. Lmberis and A. Dittmar, "Advanced wearable health systems and applications—Research and development efforts in the European Union," *IEEE Eng. Med. Biol. Mag.*, vol. 26, no. 3, pp. 29–33, May 2007.

[10] Y. Kumar *et al.*, "Wireless wearable range-of-motion sensor system for upper and lower extremity joints: a validation study," *Healthcare Technol. Lett.*, vol. 2, no. 1, pp. 12–17, 2015.

[11] J. Sakuma, D. Anzai, and J. Wang, "Performance of human body communication-based wearable ecg with capacitive coupling electrodes," *Healthcare Technol. Lett.*, vol. 3, no. 3, pp. 222–225, 2016.

[12] E. Sardini, M. Serpelloni, and V. Pasqui, "Wireless wearable t-shirt for posture monitoring during rehabilitation exercises," *IEEE Trans. Instrum. Meas.*, vol. 64, no. 2, pp. 439–448, Feb. 2015.

[13] L. M. Borges, R. Chvez-Santiago, N. Barroca, F. J. Velez, and I. Balasingham, "Radio-frequency energy harvesting for wearable sensors," *Healthcare Technol. Lett.*, vol. 2, no. 1, pp. 22–27, 2015.

[14] M. Delrobaei, N. Baktash, G. Gilmore, K. McIsaac, and M. Jog, "Using wearable technology to generate objective Parkinson's disease dyskinesia severity score: Possibilities for home monitoring," *IEEE Trans. Neural Syst. Rehabil. Eng.*, vo. PP, no. 99, p. 1, 2017.

[15] T. Wen, L. Wang, J. Gu, and B. Huang, "An acceleration-based control framework for interactive gaming," in *Proc. Annu. Int. Conf. IEEE Eng. Med. Biol. Soc.*, Sep. 2009, pp. 2388–2391.

[16] R. B. R. Manero *et al.*, "Wearable embroidered muscle activity sensing device for the human upper leg," in *Proc. 38th Annu. Int. Conf. IEEE Eng. Med. Biol. Soc.*, Aug. 2016, pp. 6062–6065.

[17] G. Robertson, G. Caldwell, J. Hamill, G. Kamen, and S. Whittlesey, *Research Methods in Biomechanics*, 2nd ed. United States: Human Kinetics, Champaign, IL 61825–5076, 2013.

[18] T. Kamali, R. Boostani, and H. Parsaei, "A multi-classifier approach to MUAP classification for diagnosis of neuromuscular disorders," *IEEE Trans. Neural Syst. Rehabil. Eng.*, vol. 22, no. 1, pp. 191–200, Jan. 2014.

[19] S. S. Nair, R. M. French, D. Laroche, and E. Thomas, "The application of machine learning algorithms to the analysis of electromyographic patterns from arthritic patients," *IEEE Trans. Neural Syst. Rehabil. Eng.*, vol. 18, no. 2, pp. 174–184, Apr. 2010.

[20] Z. Song, S. Guo, and Y. Fu, "Development of an upper extremity motor function rehabilitation system and an assessment system," *Int. J. Mechatronics Autom.*, vol. 1, no. 1, pp. 19–28, 2011.

[21] T. Kamali, R. Boostani, and H. Parsaei, "A multi-classifier approach to MUAP classification for diagnosis of neuromuscular disorders," *IEEE Trans. Neural Syst. Rehabil. Eng.*, vol. 22, no. 1, pp. 191–200, Jan. 2014.

[22] M. Nagaraju *et al.*, "Circuit techniques for wireless bioelectrical interfaces," in *Proc. Int. Symp. VLSI Des. Autom. Test*, 2010, pp. 117–120.

[23] Y. Oonishi, S. Oh, and Y. Hori, "A new control method for power-assisted wheelchair based on the surface myoelectric signal," *IEEE Trans. Ind. Electron.*, vol. 57, no. 9, pp. 3191–3196, 2010.

[24] X. Zhang, X. Chen, Y. Li, V. Lantz, K. Wang, and J. Yang, "A framework for hand gesture recognition based on accelerometer and EMG sensors," *IEEE Trans. Syst., Man, Cybern. A, Syst. Humans*, vol. 41, no. 6, pp. 1064–1076, Nov. 2011.

[25] M. Khezri and M. Jahed, "Real-time intelligent pattern recognition algorithm for surface EMG signals," *Biomed. Eng. Online*, vol. 6, no. 1, pp. 1-12–3-12, 2007.

[26] S. Benatti *et al.*, "A versatile embedded platform for EMG acquisition and gesture recognition," *IEEE Trans. Biomed. Circuits Syst.*, vol. 9, no. 5, pp. 620–630, Oct. 2015.

[27] Thalmic Labs, Kitchener, ON, Canada, "Myo: Gesture control armband website," 2017. [Online]. Available: https://www.thalmic.com/en/myo/

[28] U. Imtiaz *et al.*, "Design of a wireless miniature low cost EMG sensor using gold plated dry electrodes for biomechanics research," in *Proc. IEEE Int. Conf. Mechatronics Autom.*, Aug. 2013, pp. 957–962.

[29] R. M. Rangayyan, *Analysis of Concurrent, Coupled, and Correlated Processes*. Piscataway, NJ, USA: IEEE Press, 2015, p. 720. [Online]. Available: http://ieeexplore.ieee.org/xpl/articleDetails.jsp?arnumber=7111658

[30] M. Tomasini, S. Benatti, B. Milosevic, E. Farella, and L. Benini, "Power line interference removal for high-quality continuous biosignal monitoring with low-power wearable devices," *IEEE Sensors J.*, vol. 16, no. 10, pp. 3887–3895, May 2016.

[31] D. Farina, R. Merletti, M. Nazzaro, and I. Caruso, "Effect of joint angle on EMG variables in leg and thigh muscles," *IEEE Eng. Med. Biol. Mag.*, vol. 20, no. 6, pp. 62–71, Nov./Dec. 2001.

[32] M. Cifrek, S. Tonković, and V. Medved, "Measurement and analysis of surface myoelectric signals during fatigued cyclic dynamic contractions," *Measurement*, vol. 27, no. 2, pp. 85–92, 2000.

[33] S. Karlsson, J. Yu, and M. Akay, "Time-frequency analysis of myoelectric signals during dynamic contractions: A comparative study," *IEEE Trans. Biomed. Eng.*, vol. 47, no. 2, pp. 228–238, Feb. 2000.

[34] R. Merletti and P. Di Torino, "Standards for reporting EMG data," *J. Electromyography Kinesiol*, vol. 9, no. 1, pp. 2–3, 1999.

[35] C. J. De Luca, L. D. Gilmore, M. Kuznetsov, and S. H. Roy, "Filtering the surface EMG signal: Movement artifact and baseline noise contamination," *J. Biomech.*, vol. 43, no. 8, pp. 1573–1579, 2010.

[36] A. P. Vinod and C. Y. Da, "An integrated surface EMG data acquisition system for sports medicine applications," in *Proc. 7th Int. Symp. Med. Inf. Commun. Technol.*, Mar. 2013, pp. 98–102.

[37] M. F. Chimene and R. Pallas-Areny, "A comprehensive model for power line interference in biopotential measurements," *IEEE Trans. Instrum. Meas.*, vol. 49, no. 3, pp. 535–540, Jun. 2000.

[38] S. Santoso, R. C. Dugan, M. F. McGranaghan, and H. W. Beaty, *Electrical Power Systems Quality*. New York, NY, USA: McGraw-Hill, 2003.

[39] C. J. De Luca, L. D. Gilmore, M. Kuznetsov, and S. H. Roy, "Filtering the surface EMG signal: Movement artifact and baseline noise contamination," *J. Biomech.*, vol. 43, no. 8, pp. 1573–1579, 2010.

[40] M. Zivanovic and M. González-Izal, "Simultaneous powerline interference and baseline wander removal from ECG and EMG signals by sinusoidal modeling," *Med. Eng. Phys.*, vol. 35, no. 6, pp. 1431–1441, Mar. 2013.
[41] Biometrics Ltd, Newport, U.K., "sEMG sensor." [Online]. Available: http://www.biometricsltd.com/semg.htm
[42] Biometrics Ltd, Newport, U.K., "Datalog MWX8." [Online]. Available: http://www.biometricsltd.com/datalog.htm
[43] Delsys, Natick, MA, USA, "Trigno lab," 2017. [Online]. Available: http://www.delsys.com/products/wireless-emg/trigno-lab/
[44] M. T. Wolf *et al.*, "Decoding static and dynamic arm and hand gestures from the JPL biosleeve," in *Proc. IEEE Aerosp. Conf.*, Mar. 2013, pp. 1–9.
[45] H. Lee, K. Kim, and S. R. Oh, "Development of a wearable and dry sEMG electrode system for decoding of human hand configurations," in *Proc. IEEE/RSJ Int. Conf. Intell. Robots Syst.*, Oct. 2012, pp. 746–750.
[46] X. Tang, Y. Liu, C. Lv, and D. Sun, "Hand motion classification using a multi-channel surface electromyography sensor," *Sensors*, vol. 12, no. 2, pp. 1130–1147, 2012.
[47] Y. Fang, X. Zhu, and H. Liu, "Development of a surface EMG acquisition system with novel electrodes configuration and signal representation," in *Proceedings of the 6th International Conference on Intelligent Robotics and Applications*, vol. 8102. New York, NY, USA: Springer-Verlag, 2013, pp. 405–414. [Online]. Available: http://dx.doi.org/10.1007/978-3-642-40852-6_41
[48] G. Imperatori, P. Cunzolo, D. Cvetkov, and D. Barrettino, "Wireless surface electromyography probes with four high-speed channels," *IEEE Sensors J.*, vol. 13, no. 8, pp. 2954–2961, Aug. 2013.
[49] D. T. Mewett, H. Nazeran, and K. J. Reynolds, "Removing power line noise from recorded EMG," in *Proc. 23rd Annu. Int. Conf. IEEE Eng. Med. Biol. Soc.*, 2001, vol. 3, pp. 2190–2193.
[50] M. Malboubi, F. Razzazi, and S. M. Aliyari, "Elimination of power line noise from EMG signals using an efficient adaptive Laguerre filter," in *Proc. Int. Conf. Signals Electron. Circuits*, Sep. 2010, pp. 49–52.
[51] M. R. Keshtkaran and Z. Yang, "A robust adaptive power line interference canceler VLSI architecture and ASIC for multichannel biopotential recording applications," *IEEE Trans. Circuits Syst. II, Express Briefs*, vol. 61, no. 10, pp. 788–792, Oct. 2014.
[52] S. Suppappola and Y. Sun, "Nonlinear transforms of ECG signals for digital QRS detection: A quantitative analysis," *IEEE Trans. Biomed. Eng.*, vol. 41, no. 4, pp. 397–400, Apr. 1994.
[53] B. McCarthy, K. Stephens, C. King, E. Chabot, and Y. Sun, "Graded muscle contractions determined by temporal recruitment," in *Proc. 40th Annu. Northeast Bioeng. Conf.*, Apr. 2014, pp. 1–2.
[54] M. Okada, "A digital filter for the ORS complex detection," *IEEE Trans. Biomed. Eng.*, vol. BME-26, no. 12, pp. 700–703, Dec. 1979.
[55] P. S. Hamilton and W. J. Tompkins, "Quantitative investigation of QRS detection rules using the MIT/BIH arrhythmia database," *IEEE Trans. Biomed. Eng.*, vol. BME-33, no. 12, pp. 1157–1165, Dec. 1986.
[56] A. Merlo, D. Farina, and R. Merletti, "A fast and reliable technique for muscle activity detection from surface EMG signals," *IEEE Trans. Biomed. Eng.*, vol. 50, no. 3, pp. 316–323, Mar. 2003.
[57] Q. Xu, Y. Quan, L. Yang, and J. He, "An adaptive algorithm for the determination of the onset and offset of muscle contraction by EMG signal processing," *IEEE Trans. Neural Syst. Rehabil. Eng.*, vol. 21, no. 1, pp. 65–73, Jan. 2013.
[58] B. Hudgins, P. Parker, and R. N. Scott, "A new strategy for multifunction myoelectric control," *IEEE Trans. Biomed. Eng.*, vol. 40, no. 1, pp. 82–94, Jan. 1993.
[59] A. Phinyomark, P. Phukpattaranont, and C. Limsakul, "Fractal analysis features for weak and single-channel upper-limb EMG signals," *Expert Syst. Appl.*, vol. 39, no. 12, pp. 11156–11163, 2012.
[60] F. Garavito, J. Gonzalez, J. Cabarcas, D. Chaparro, I. Portocarrero, and A. Vargas, "EMG signal analysis based on fractal dimension for muscle activation detection under exercice protocol," in *Proc. 21st Symp. Signal Process., Images Artif. Vis.*, Aug. 2016, pp. 1–5.
[61] G. Naik, D. Kumar, and S. Arjunan, "Pattern classification of Myoelectrical signal during different maximum voluntary contractions: A study using BSS techniques," *Meas. Sci. Rev.*, vol. 10, no. 1, pp. 1–6, 2010.
[62] R. Atri *et al.*, "Investigation of muscle activity during loaded human gait using signal processing of multi-channel surface EMG and IMU," in *Proc. IEEE Signal Process. Med. Biol. Symp.*, Dec. 2016, pp. 1–6.
[63] S. Pasinetti, M. Lancini, I. Bodini, and F. Docchio, "A novel algorithm for EMG signal processing and muscle timing measurement," *IEEE Trans. Instrum. Meas.*, vol. 64, no. 11, pp. 2995–3004, Nov. 2015.
[64] C. Zizoua, M. Raison, S. Boukhenous, M. Attari, and S. Achiche, "Detecting muscle contractions using strain gauges," *Electron. Lett.*, vol. 52, no. 22, pp. 1836–1838, 2016.
[65] J. Luan, S. Lee, and P. H. Chou, "Low-power detection of sternocleidomastoid muscle contraction for asthma assessment and control," in *Proc. IEEE/ACM Int. Symp. Low Power Electron. Des.*, Jul. 2015, pp. 183–188.
[66] R. A. Serway, *Principles of Physics*. Brooks/Cole–Thomson Learning 10 Davis Drive Belmont, CA 94002-3098 USA, 1998.
[67] SENIAM, Enschede, The Netherlands, "Sensor placement," 2017. [Online]. Available: http://www.seniam.org/bicepsbrachii.html
[68] E. Vavrinskỳ *et al.*, "Design of EMG wireless sensor system," in *Proc. Int. Conf. Appl. Electron.*, 2011, pp. 1–4.
[69] J. Xu, R. F. Yazicioglu, B. Grundlehner, P. Harpe, K. A. A. Makinwa, and C. V. Hoof, "A 160 mu 8-channel active electrode system for EEG monitoring," *IEEE Trans. Biomed. Circuits Syst.*, vol. 5, no. 6, pp. 555–567, Dec. 2011.

Mert Ergeneci received the Diploma in electrical and electronics engineering from Bilkent University, Ankara, Turkey, in 2016. He is a cofounder of Hercules Biomedical R&D, a research and development company funded by Scientific and Technological Research Council of Turkey, focusing on developing a wearable product to make elite athlete performance analysis and injury predictions through sensors. His research interests include biomedical data analysis, adaptive filtering, and wearable electronics.

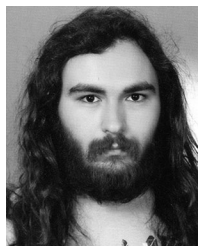

Kaan Gokcesu received the B.S. and M.S. degrees in electrical and electronics engineering from Bilkent University, Ankara, Turkey, in 2015 and 2017, respectively, and is currently working toward the Ph.D. degree in electrical engineering at Massachusetts Institute of Technology, Cambridge, MA, USA. His research interests include sequential learning, adaptive filtering, and biomedical signal processing.

Erhan Ertan received the Diploma in electrical and electronics engineering from Bilkent University, Ankara, Turkey, in 2016. He is a cofounder of Hercules Biomedical R&D, a research and development company funded by Scientific and Technological Research Council of Turkey, focusing on developing a wearable product to make elite athlete performance analysis and injury predictions through sensors. His research interest include sensor circuitry and filter designs.

Panagiotis Kosmas (M'05–SM'14) received the Diploma in electrical and computer engineering from the National Technical University of Athens, Athens, Greece, in 1999, and the M.S. and Ph.D. degrees in electrical and computer engineering from Northeastern University, Boston, MA, USA, in 2002 and 2005, respectively. In 2008, he joined King's College London (KCL), London, U.K., as a Lecturer, and is currently a Senior Lecturer in the Department of Informatics, KCL. Prior to his appointment at KCL, he held research positions at the Center for Subsurface Sensing and Imaging Systems, Boston, MA, USA, the University of Loughborough, Loughborough, U.K., and the Computational Electromagnetics Group, University of Wisconsin-Madison, Madison, WI, USA. He is also a cofounder of Mediwise Ltd, an award-winning U.K.-based SME focusing on the use of electromagnetic waves for medical applications. He is an elected Working Group Leader for COST Action MiMed (TD1301), Development of a European-based Collaborative Network to Accelerate Technological, Clinical and Commercialisation Progress in the area of medical microwave imaging. His research interests include computational electromagnetics with application to sensing and imaging, antenna design, physics-based detection methods, and inverse problems theory and techniques.